

Spin and orbital Hall currents detected via current induced magneto-optical Kerr effect in V and Pt

Yukihiro Marui,¹ Masashi Kawaguchi,¹ Satoshi Sumi,²
Hiroyuki Awano,² Kohji Nakamura,³ and Masamitsu Hayashi^{1,4}

¹*Department of Physics, The University of Tokyo, Tokyo, 113-0033, Japan*

²*Toyota Technological Institute, Nagoya, 468-8511, Japan*

³*Department of Physics Engineering, Mie University, Tsu, 514-8507, Japan*

⁴*Trans-scale quantum science institute, The University of Tokyo, Tokyo, 113-0033, Japan*

(Dated: June 19, 2023)

We have studied the film thickness dependence of current induced magneto-optical Kerr effect in Pt and V thin films. The Kerr signal for Pt shows little dependence on the thickness in the range studied (20-80 nm). In contrast, the signal for V increases with increasing thickness and saturates at a thickness near 100 nm to a value significantly larger than that of Pt. These experimental results are accounted for assuming that spin and orbital Hall effects are responsible for the Kerr signal. We show that the Kerr signal is proportional to the product of the dc spin (orbital) Hall conductivity and the energy derivative of the ac spin (orbital) Hall conductivity. Contributions from the spin and orbital Hall effects add up for V whereas they cancel out for Pt. The thickness dependence of the Kerr signal suggests that the orbital diffusion length of V is considerably smaller compared to its spin diffusion length.

Efficient generation of spin current is one of the key challenges in developing random access and storage class memory technologies[1, 2]. The spin Hall effect[3, 4] of the *5d* transition metals is considered as, by far, the most viable approach in generating spin current using materials that are compatible with semiconductor manufacturing processes[5]. The efficiency to generate spin current is often represented by the spin Hall angle of the host material. The spin Hall angle is proportional to the product of the spin Hall conductivity and the resistivity. With regard to technological applications, it is preferable to reduce the resistivity for limiting power consumption. Therefore, significant effort has been placed to find/develop materials with large spin Hall conductivity.

It has been shown that, in the *5d* transition metals, the spin Hall conductivity is determined by its band structure and/or spin dependent scattering[6]. The latter, often referred to as the extrinsic spin Hall effect, can enhance the spin Hall conductivity if appropriate element is doped as a scattering center[7, 8]. The former, i.e. the intrinsic spin Hall effect, is determined by the electronic structure of the host material[9]. Studies have shown that the spin Hall conductivity of transition metals follows a Hund's rule-like scaling and is proportional to the $\mathbf{L} \cdot \mathbf{S}$ spin orbit coupling, where \mathbf{S} and \mathbf{L} are the total spin and orbital angular momentum of the host element[10]. Such trend has been found in experiments[11, 12], suggesting that the intrinsic spin Hall effect is relevant to generating spin current in non-doped transition metals.

Theoretical studies on the intrinsic spin Hall effect have proposed that the spin current is accompanied by a flow of orbital angular momentum, referred to as the orbital current, generated by the orbital Hall effect[10, 13, 14]. Orbital current consists of flow of electrons with opposite orbital angular momentum moving in opposite directions. In contrast to the spin Hall conductivity, the orbital Hall conductivity is predicted to be independent

of the size and sign of the spin orbit coupling ($\mathbf{L} \cdot \mathbf{S}$). Using tight binding and/or first principle calculations, it has been shown that the *3d* transition metals, V, Ti and Cr in particular, possess one of the largest orbital Hall conductivities among the transition metals[10, 15, 16].

Probing the orbital current remains a significant challenge in modern Spintronics. A large number of studies have used bilayers that consist of a non-magnetic metal (NM) and a ferromagnetic metal (FM) to assess the presence of orbital current. In almost all cases, the response of the FM layer magnetization to the current passed along the bilayer is used to study the size and direction of orbital current, if any, generated in the NM layer[17–21]. There are a few difficulties in evaluating the orbital current in such systems. First, as many studies use the change in the magnetization direction with the current to extract information on the orbital current, it is essential that the orbital current exerts torque on the magnetization. However, it remains to be seen if the orbital current that enters the FM layer can exert torque on the FM layer magnetization in a way similar to that of spin current (see e.g. Refs. [22, 23]). Second, it is well known that the electronic and/or structural properties of the NM/FM interface can significantly influence the amplitude and the direction of spin current that flows into the FM layer[24–27]. The same issue also applies to orbital current. Finally, studies have shown that the presence of the FM layer can alter the spin transport properties within the NM layer via a proximity-like effect. For example, the spin diffusion length of the NM layer has been reported to differ depending on whether or not a FM layer is placed adjacent to the NM layer[28]. Similar effects may also apply to the orbital current in the NM layer. For these reasons, it is preferable to probe the orbital current, if any, in a single NM layer.

The first observation of the spin Hall effect used the magneto-optical Kerr effect in the polar configuration to

detect the amount of out of plane spin magnetic moments accumulated at the edges of a semiconductor[29]. This was made possible partly due to the large spin diffusion length (of the order of a few μm) of the host material (GaAs). Later on, current induced spin magnetic moment, polarized along the film plane and accumulated at the surface of a NM layer, was probed using the longitudinal Kerr effect[30–33]. The change in the Kerr rotation angle induced by spin magnetic moment was of the order of nano-radian. As the effect is not limited to detecting spin magnetic moment, one may probe orbital magnetic moment at the surface/edges of non-magnetic materials[34].

Here we use the longitudinal magneto-optical Kerr effect to study current induced spin and orbital magnetic moments in NM single layer films. We compare the Kerr signal of Pt, known for its large spin Hall conductivity, and V, which is predicted to exhibit a large orbital Hall conductivity. A simple model is developed to analyze the experimental results. We show that the real and imaginary parts of the Kerr signal can be used to determine the spin and orbital Hall effects of the host material. From the analyses, we determine the spin and orbital diffusion length of Pt and V.

Films are deposited using RF magnetron sputtering on thermally oxidized silicon substrates (the SiO_2 thickness is ~ 100 nm). The film structure is sub./t NM/2 MgO/1 Ta (thickness in units of nanometer) where NM = Pt, V. Optical lithography and Ar ion milling are used to pattern the films into a wire. The width and length of the wire are 0.4 mm and 1.2 mm, respectively. Electrodes made of 5 Ta/60 Cu/3 Pt are formed using conventional liftoff techniques. X-ray diffraction is used to study the film structure. For V, we find the bcc (110) peak in the 20-nm-thick V thin film, suggesting that the film is composed of bcc-V.

Schematic illustration of the experimental setup is shown in Fig. 1. An alternating current is applied to

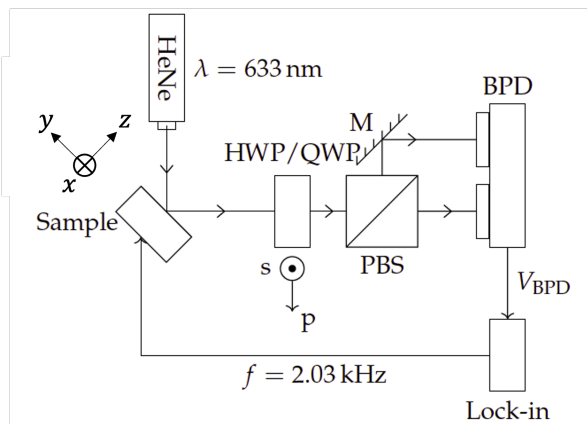


Figure 1: Schematic illustration of the optical setup. Definition of the coordinate system and the polarization of the light are shown.

the sample. The frequency of the current is fixed to 2030 Hz and the amplitude is varied. The sample is irradiated with a linearly polarized light from an oblique angle (~ 45 deg from the film normal). The light plane of incidence is parallel to the current flow direction. The reflected light is measured using a balanced photodetector, where the optical signal is converted to an electrical signal. The electrical output of the photodetector is fed into a lock-in amplifier. The frequency and phase of the lock-in amplifier are locked to those of the alternating current applied to the sample. A half wave plate is inserted in between the sample and the photodetector. The optical axis of the half wave plate is varied to measure the real (θ_K , rotation angle) and imaginary (η_K , ellipticity) parts of the Kerr rotation angle. θ_K and η_K are measured as a function of the current density j applied to the sample. Such measurement is repeated N times to improve the signal to noise ratio (typical $N = 100 - 1000$).

The j dependence of θ_K and η_K are shown in Fig. 2 for 20 nm thick Pt and V films. Positive and negative j correspond to, respectively, in-phase and (180 deg) out-of-phase detection of the optical signal with respect to the current. We find that both θ_K and η_K linearly scales with j at small $|j|$. Data is fitted with a linear function to obtain the rate at which the Kerr signal varies with j . Note that a slight non-linear j dependence of the Kerr signal is found when $|j|$ exceeds 1×10^{10} A/m^2 ; see, for example, Fig. 2(a). We thus limit the data fitting range to below such value. The film thickness dependence of θ_K/j and η_K/j obtained from the linear fitting are presented in Fig. 3 with the open symbols. For Pt, we find that both θ_K/j and η_K/j show relatively little dependence on the Pt layer thickness. In contrast, θ_K/j for V steadily

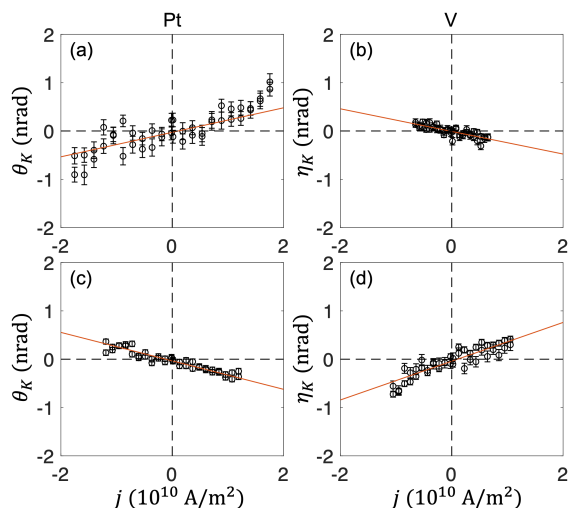


Figure 2: (a-d) Current density j dependence of the real part θ_K (a,c) and the imaginary part η_K (b,d) of the Kerr signal. Data are from 20 nm Pt (a,b) and 20 nm V (c,d). The error bars indicate standard deviation of the N measurements conducted normalized by $\sqrt{N - 1}$.

increases with increasing V layer thickness (η_K/j shows a rather small variation). The absolute value of the Kerr signal $|\theta_K + i\eta_K|/j$ is plotted in Fig. 3(b). As evident, the absolute Kerr signal is significantly larger for V than Pt in the thick NM layer limit.

To account for these experimental results, we model the current induced magneto-optical Kerr effect assuming that spin and orbital magnetic moments, induced by spin and orbital Hall effects, respectively, accumulate at the surface of the film. θ_K and η_K are defined using the reflection coefficients r_{ss} and r_{ps} :

$$\theta_K = \text{Re} \left[\frac{r_{ps}}{r_{ss}} \right], \quad \eta_K = \text{Im} \left[\frac{r_{ps}}{r_{ss}} \right], \quad (1)$$

where $r_{ss(p)}$ represents the fraction of the s (p) component of the reflected light when a sample is irradiated with an s -polarized light. (The same convention applies when the sample is irradiated with a p -polarized light.) r_{ss} (r_{ps}) can be expressed using the diagonal (ϵ_{xx}) and

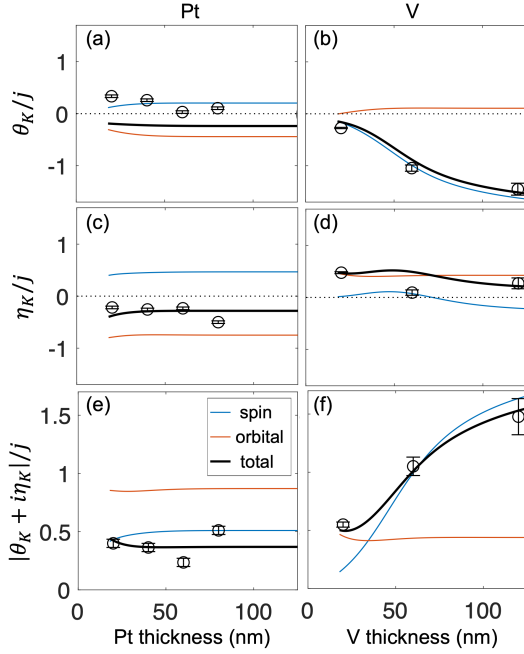


Figure 3: (a-f) The NM layer thickness dependence of the real part θ_K/j (a,b), the imaginary part η_K/j (c,d) and the absolute value $|\theta_K + i\eta_K|/j$ (e,f) of the Kerr signal divided by the current density j . The circles show experimental data from Pt (a,c,e) and V (b,d,f). The error bars represent fitting error of the j dependence of the Kerr signal with a linear function. Blue, red and black lines show calculated Kerr signal with contribution from the spin Hall effect, orbital Hall effect and the sum of the two, respectively. Parameters used in the calculations are summarized in Table I. Calculation results for the thin NM layer limit are not shown for clarity: see Materials and Methods ?? and Fig. S3 for the details.

off-diagonal (e.g. ϵ_{zx}) components of the permittivity tensor for each layer and geometrical parameters of the experimental setup (e.g. the light incident angle). For a sample made of non-magnetic materials, ϵ_{zx} is generally zero, which results in $r_{ps} = 0$. Under the influence of spin and orbital Hall effects, current applied to the sample induces non-zero spin and/or orbital magnetic moments at the top and bottom surfaces of the film.

We use the spin diffusion equation[35] to obtain the profile of the spin/orbital magnetic moment. Following the approach described in Materials and Methods ??, ϵ_{zx} reads

$$\epsilon_{zx} = \epsilon_{zx,s} + \epsilon_{zx,o},$$

$$\epsilon_{zx,s(o)} = -\frac{el_{s(o)}\rho_{xx}^2\sigma_{s(o)}(0)}{\epsilon_0\omega} \frac{\sinh\left(\frac{t-2z}{2l_{s(o)}}\right)}{\cosh\left(\frac{t}{2l_{s(o)}}\right)} \frac{\partial\sigma_{s(o)}(\omega)}{\partial E}, \quad (2)$$

where ϵ_0 is the vacuum permittivity, e is the electric charge, ω is the light angular frequency, σ_{xx} , $\sigma_{s(o)}(0)$, $l_{s(o)}$ are the conductivity, dc spin (orbital) Hall conductivity and the spin (orbital) diffusion length, respectively, of the NM layer. $\sigma_{s(o)}(\omega)$ is the NM layer ac spin (orbital) Hall conductivity at light angular frequency ω and $\frac{\partial\sigma_{s(o)}(\omega)}{\partial E}$ is its energy derivative taken at the Fermi level. $z = 0$ and $z = t$ correspond to bottom (facing the substrate) and top surfaces of the NM layer, respectively.

The Kerr signal is computed numerically. Since ϵ_{zx} varies along the film thickness, the NM layer is divided into sub-layers with a thickness of δt and a constant ϵ_{zx} . Here we set $\delta t = 0.1$ nm. We neglect the effect of the capping layer (2 MgO/1 Ta) as it is transparent to visible light (the top Ta layer is oxidized due to exposure to air). Following Zak *et al.*[36], we compute the 4×4 boundary A_j and propagation D_j matrices for each (sub)layer j . The reflection coefficients can be expressed as

$$M = A_a^{-1} \prod_n (A_n D_n A_n^{-1}) (A_o D_o A_o^{-1}) A_s = \begin{bmatrix} G & H \\ J & K \end{bmatrix},$$

$$\begin{bmatrix} r_{ss} & r_{sp} \\ r_{ps} & r_{pp} \end{bmatrix} = JG^{-1}, \quad (3)$$

where G , H , J and K are 2×2 matrices. A_a , A_n (D_n), A_o (D_o) and A_s are the boundary (propagation) matrices for air, NM layer, SiO_2 layer and the Si substrate, respectively. Note that both A_n and D_n contain ϵ_{zx} of the NM layer. Detailed form of the matrices are described in the Materials and Methods ??.

We first show in Fig. 4 representative calculation results using general parameters. To simplify the modeling, we neglect the SiO_2 layer of the substrate, which can influence the Kerr signal due to multiple reflection within SiO_2 when the NM layer is thin. The red and blue lines in Fig. 4 represent contributions from the spin and orbital Hall effects to the Kerr signal. The solid and dashed lines in Fig. 4(a,b) show θ_K and η_K , whereas the solid lines in Fig. 4(c,d) represent the absolute value $|\theta_K + i\eta_K|$. The thick black line in Fig. 4(c,d) show the sum from the two

(spin and orbit) contributions. Parameters used in the calculations are summarized in the forth and fifth lines of Table I.

In Fig. 4, all parameters are fixed except for the sign of $\frac{\partial\sigma_o(\omega)}{\partial E}$, which is opposite between Fig. 4(a,c) and 4(b,d). As evident, $|\theta_K + i\eta_K|$ in the thick NM limit is significantly larger for Fig. 4(d) than Fig. 4(b). Equation (2) shows that the Kerr signal scales with the sum of contributions from the spin and orbital Hall effects, each of which is proportional to the product of the dc spin/orbital Hall conductivity and the energy derivative of the ac spin/orbital Hall conductivity (i.e. Kerr signal $\propto \sigma_s(0)\frac{\partial\sigma_s(\omega)}{\partial E} + \sigma_o(0)\frac{\partial\sigma_o(\omega)}{\partial E}$). If the sign of the product is the same (opposite) for spin and orbital Hall effects, both contributions add up (cancel out), which is the case for Fig. 4(b,d) [Fig. 4(a,c)]. As we show below, contributions from spin and orbital Hall effects cancel out for Pt whereas they add up for V.

We use the model to describe the experimental results. Here we include the SiO₂ layer in the calculations. ϵ_{xx} for the NM layer and the substrate is obtained from standard ellipsometry measurements (see Materials and Methods??). The NM layer resistivity is measured with four point probe technique. The dc and ac spin Hall conductivities are calculated using first principles calculations. Details of the calculations are described in Materials and Methods. The spin (l_s) and orbital (l_o) diffusion length are used as fitting parameters to account for the data presented in Fig. 3, open symbols. For V, we slightly adjust the dc and ac spin Hall conductivities to

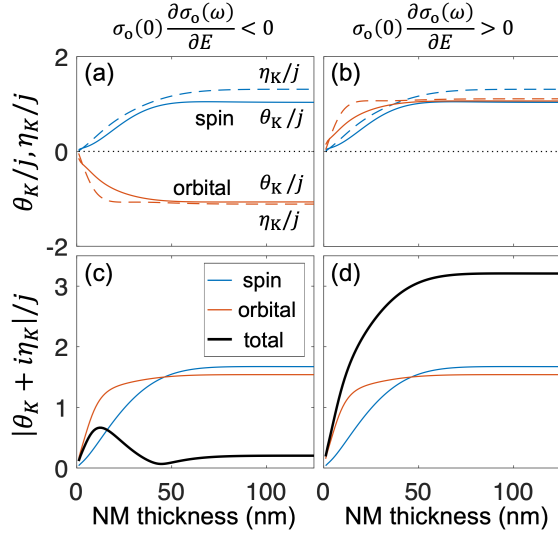


Figure 4: (a-d) The NM layer thickness dependence of the calculated θ_K (solid line), η_K (dashed line) (a,b) and the calculated $|\theta_K + i\eta_K|/j$ (c,d). Blue, red and black lines show contribution from the spin Hall effect, orbital Hall effect and the sum of the two, respectively. Parameters used in the calculations are shown in the 4th and 5th lines of Table I.

fit the data. (As the dc and ac spin Hall conductivity of V are small, we consider the accuracy of the calculations is smaller than that of Pt and the orbital Hall conductivity of V). The parameters used in the calculations are summarized in Table I (first and second lines). The third line of Table I shows the dc and ac spin Hall conductivities from first principles calculations. Note that the fitted value of the dc spin Hall conductivity $\sigma_s(0) \sim 154$ ($\Omega \cdot \text{cm}$)⁻¹ is close to what has been found experimentally for bcc-V ($\sigma_s(0) \sim 200$ ($\Omega \cdot \text{cm}$)⁻¹)[37].

The model calculation results are shown by the solid lines in Fig. 3. The red and blue lines represent contributions from the spin and orbital Hall effects to the Kerr signal whereas the thick black line shows the sum of the two. We find good agreement between the experimental results and the calculations. First, the calculations reproduce the relative magnitude of the Kerr signal of Pt and V found in the experiments. First principles calculations suggest that the signs of $\sigma_s(0)\frac{\partial\sigma_s(\omega)}{\partial E}$ and $\sigma_o(0)\frac{\partial\sigma_o(\omega)}{\partial E}$ are opposite for Pt while they are the same for V (see Table I). From the model calculations, this suggests that the spin and orbital Hall contributions cancel out for Pt whereas they both positively contribute for V. Second, we find in the experiments that the Kerr signal increases with increasing V thickness and tends to saturate at $d \sim 100$ nm. This suggest that l_s and/or l_o have a length scale of the order of a few tens of nm. Note that the spin/orbital diffusion length also sets the magnitude of the Kerr signal. Given the large orbital Hall conductivity of V estimated from first principles calculations, l_o must be smaller than ~ 1 nm in order to describe the Kerr signal found in the experiments. We thus consider l_o of V is significantly smaller than l_s . Finally, as presented in Fig. 3(d), a large fraction of V Kerr signal is induced by the spin Hall effect due to the large l_s . One may consider whether all the V Kerr signal can be accounted for with the spin Hall effect if we further increase the dc and ac spin Hall conductivities. We find that the overall thickness dependence of the Kerr signal cannot be accounted for with a single diffusion length: one needs a short and a long diffusion lengths to describe the experimental results. These results thus suggest that the orbital Hall effect plays a role in generating magnetic moment at the film surface.

In summary, we have studied current induced magneto-optical Kerr effect in Pt and V thin films. We find the Kerr signal of V is significantly larger than that of Pt when the film thickness is ~ 100 nm. A model, developed to account for the experimental results, suggests that the Kerr signal is proportional to the sum of contributions from the spin and orbital Hall effects, each of which is proportional to the product of the dc spin/orbital Hall conductivity and the energy derivative of the ac spin/orbital Hall conductivity. We find contributions from the spin and orbital Hall effects cancel out for Pt whereas the two effects add up for V, leading to a larger signal for the latter. The analyses suggest that the

Table I: Parameters used in the model calculations. The first and second (forth and fifth) lines show parameters for which the results are presented in Fig. 3 (Fig. 4). The third line represents parameters obtained using first principles calculations for V. The light frequency ω corresponds to that of $\lambda = 633$ nm.

	$\sigma_s(0)$ $(\Omega \cdot \text{cm})^{-1}$	l_s nm	$\frac{\partial \sigma_s(\omega)}{\partial E}$ $(\Omega \cdot \text{cm eV})^{-1}$	$\sigma_o(0)$ $(\Omega \cdot \text{cm})^{-1}$	l_o nm	$\frac{\partial \sigma_o(\omega)}{\partial E}$ $(\Omega \cdot \text{cm eV})^{-1}$	ρ_{xx} $\mu\Omega \text{ cm}$	n
Pt	2078	4.0	$314 + 1540i$	3240	2.0	$-1620 - 5670i$	17	$1.77 + 4.33i$
V	-154	40	$160 - 290i$	4180	0.7	$1770 + 1280i$	41	$2.91 + 3.26i$
V(DFT)	-53	n/a	$-16 - 101i$	4180	n/a	$1770 + 1280i$	n/a	n/a
Fig. 4(a)	1000	10	$1000 + 1000i$	2000	4	$-2000 - 2000i$	20	$2 + 4i$
Fig. 4(b)	1000	10	$1000 + 1000i$	2000	4	$2000 + 2000i$	20	$2 + 4i$

orbital diffusion length of V must be significantly smaller than the spin diffusion length, provided that the magnitude of the orbital Hall conductivity is close to what first principles calculations predict. These results thus clarify the mechanism of current induced magneto-optical Kerr effect in metallic thin films.

Acknowledgements: This work was partly supported by JSPS KAKENHI (Grant Numbers 23H00176, 20J13860), JST CREST (JPMJCR19T3), MEXT Initiative to Establish Next-generation Novel Integrated Circuits Centers (X-NICS) and Cooperative Research Project Program of RIEC, Tohoku University.

-
- [1] S. Parkin and S. H. Yang, *Nat. Nanotechnol.* **10**, 195 (2015).
- [2] B. Dieny, I. L. Prejbeanu, K. Garello, P. Gambardella, P. Freitas, R. Lehdorff, W. Raberg, U. Ebels, S. O. Demokritov, J. Akerman, A. Deac, P. Pirro, C. Adelmann, A. Anane, A. V. Chumak, A. Hirohata, S. Mangin, S. O. Valenzuela, M. C. Onbasli, M. D’Aquino, G. Prenat, G. Finocchio, L. Lopez-Diaz, R. Chantrell, O. Chubykalo-Fesenko, and P. Bortolotti, *Nat. Electron.* **3**, 446 (2020).
- [3] M. I. Dyakonov and V. I. Perel, *JETP Lett.* **13**, 467 (1971).
- [4] S. Murakami, N. Nagaosa, and S. C. Zhang, *Science* **301**, 1348 (2003).
- [5] A. Hoffmann, *IEEE Trans. Magn.* **49**, 5172 (2013).
- [6] J. Sinova, S. O. Valenzuela, J. Wunderlich, C. H. Back, and T. Jungwirth, *Rev. Mod. Phys.* **87**, 1213 (2015).
- [7] Y. Niimi, M. Morota, D. H. Wei, C. Deranlot, M. Basletic, A. Hamzic, A. Fert, and Y. Otani, *Phys. Rev. Lett.* **106**, 126601 (2011).
- [8] E. Sagasta, Y. Omori, S. Velez, R. Llopis, C. Tollan, A. Chuvilin, L. E. Hueso, M. Gradhand, Y. Otani, and F. Casanova, *Phys. Rev. B* **98**, 060410 (2018).
- [9] G. Y. Guo, S. Murakami, T. W. Chen, and N. Nagaosa, *Phys. Rev. Lett.* **100**, 096401 (2008).
- [10] T. Tanaka, H. Kontani, M. Naito, T. Naito, D. S. Hirashima, K. Yamada, and J. Inoue, *Phys. Rev. B* **77**, 165117 (2008).
- [11] M. Morota, Y. Niimi, K. Ohnishi, D. H. Wei, T. Tanaka, H. Kontani, T. Kimura, and Y. Otani, *Phys. Rev. B* **83**, 174405 (2011).
- [12] J. Liu, T. Ohkubo, S. Mitani, K. Hono, and M. Hayashi, *Appl. Phys. Lett.* **107**, 232408 (2015).
- [13] H. Kontani, T. Tanaka, D. S. Hirashima, K. Yamada, and J. Inoue, *Phys. Rev. Lett.* **102**, 016601 (2009).
- [14] D. Go, D. Jo, C. Kim, and H. W. Lee, *Phys. Rev. Lett.* **121**, 086602 (2018).
- [15] D. Jo, D. Go, and H. W. Lee, *Phys. Rev. B* **98**, 214405 (2018).
- [16] L. Salemi and P. M. Oppeneer, *Phys. Rev. Mater.* **6**, 095001 (2022).
- [17] S. Lee, M. G. Kang, D. Go, D. Kim, J. H. Kang, T. Lee, G. H. Lee, J. Kang, N. J. Lee, Y. Mokrousov, S. Kim, K. J. Kim, K. J. Lee, and B. G. Park, *Commun. Phys.* **4**, 234 (2021).
- [18] G. Sala and P. Gambardella, *Physical Review Research* **4**, 033037 (2022).
- [19] A. Bose, F. Kammerbauer, R. Gupta, D. Go, Y. Mokrousov, G. Jakob, and M. Klaui, *Phys. Rev. B* **107**, 134423 (2023).
- [20] S. Dutta and A. A. Tulapurkar, *Phys. Rev. B* **106**, 184406 (2022).
- [21] H. Hayashi, D. Jo, D. Go, T. H. Gao, S. S. Haku, Y. Mokrousov, H. W. Lee, and K. Ando, *Commun. Phys.* **6**, 32 (2023).
- [22] D. Go and H. W. Lee, *Physical Review Research* **2**, 013177 (2020).
- [23] D. Lee, D. Go, H. J. Park, W. Jeong, H. W. Ko, D. Yun, D. Jo, S. Lee, G. Go, J. H. Oh, K. J. Kim, B. G. Park, B. C. Min, H. C. Koo, H. W. Lee, O. Lee, and K. J. Lee, *Nat. Commun.* **12**, 6710 (2021).
- [24] M. D. Stiles and A. Zangwill, *Phys. Rev. B* **66**, 014407 (2002).
- [25] P. M. Haney, H. W. Lee, K. J. Lee, A. Manchon, and M. D. Stiles, *Phys. Rev. B* **87**, 174411 (2013).
- [26] J. C. Rojas-Sanchez, N. Reyren, P. Laczkowski, W. Savero, J. P. Attane, C. Deranlot, M. Jamet, J. M. George, L. Vila, and H. Jaffres, *Phys. Rev. Lett.* **112**, 106602 (2014).
- [27] W. Zhang, W. Han, X. Jiang, S.-H. Yang, and S. S. P. Parkin, *Nature Physics* **11**, 496 (2015).
- [28] L. Liu, R. A. Buhrman, and D. C. Ralph, “Review and analysis of measurements of the spin hall effect in platinum,” (2011).
- [29] Y. K. Kato, R. C. Myers, A. C. Gossard, and D. D. Awschalom, *Science* **306**, 1910 (2004).
- [30] O. M. J. van’t Erve, A. T. Hanbicki, K. M. McCreary, C. H. Li, and B. T. Jonker, *Appl. Phys. Lett.* **104**,

- 172402 (2014).
- [31] P. Riego, S. Velez, J. M. Gomez-Perez, J. A. Arregi, L. E. Hueso, F. Casanova, and A. Berger, *Appl. Phys. Lett.* **109**, 172402 (2016).
- [32] Y. D. Su, H. Wang, J. Li, C. S. Tian, R. Q. Wu, X. F. Jin, and Y. R. Shen, *Appl. Phys. Lett.* **110**, 042401 (2017).
- [33] C. Stamm, C. Murer, M. Berritta, J. Feng, M. Gabureac, P. M. Oppeneer, and P. Gambardella, *Phys. Rev. Lett.* **119**, 087203 (2017).
- [34] Y.-G. Choi, D. Jo, K.-H. Ko, D. Go, K.-H. Kim, H. G. Park, C. Kim, B.-C. Min, G.-M. Choi, and H.-W. Lee, “Observation of the orbital hall effect in a light metal ti,” (2021), arXiv:2109.14847 [cond-mat.mes-hall].
- [35] P. C. van Son, H. van Kempen, and P. Wyder, *Phys. Rev. Lett.* **58**, 2271 (1987).
- [36] J. Zak, E. R. Moog, C. Liu, and S. D. Bader, *J. Magn. Magn. Mater.* **89**, 107 (1990).
- [37] T. Wang, W. Wang, Y. Xie, M. A. Warsi, J. Wu, Y. Chen, V. O. Lorenz, X. Fan, and J. Q. Xiao, *Scientific Reports* **7**, 1306 (2017).